

## Effect of $\alpha$ -transfer polarization potential in the $^{24}\text{Mg} + ^{16}\text{O}$ system

R. Lichtenthaler Filho, A. Lepine-Szily, A. C. C. Villari, and O. Portezan Filho

*Instituto de Fısica, Universidade de Sao Paulo, 01498 Sao Paulo, Sao Paulo, Brazil*

(Received 30 December 1987)

The effect of the dynamic  $\alpha$ -transfer polarization potential on several channels of the system  $^{24}\text{Mg} + ^{16}\text{O}$  has been calculated and compared to our experimental data and those of Paul and collaborators. The general agreement is good, indicating that the  $\alpha$ -transfer coupling can have an important contribution to explain the back-angle anomalies observed in the elastic, inelastic, and transfer channels.

### I. INTRODUCTION

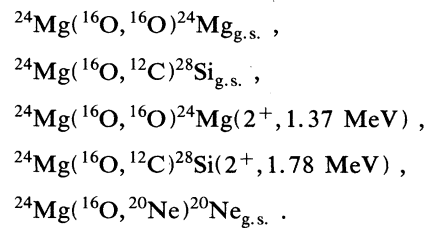
The anomalous back-angle elastic scattering of  $n\alpha$ -type nuclei ( $^{16}\text{O} + ^{28}\text{Si}$ ,  $^{16}\text{O} + ^{24}\text{Mg}$ ,  $^{12}\text{C} + ^{28}\text{Si}$ ,  $^{12}\text{C} + ^{24}\text{Mg}$ , etc.) has attracted considerable attention in the last decade.<sup>1,2</sup> The transfer reactions ( $^{16}\text{O}$ ,  $^{12}\text{C}$ ) involving these systems also present anomalous back-angle behavior, with strongly oscillating backward rise in angular distributions and very structured excitation functions at forward and backward angles.<sup>3,4</sup> A number of models have been proposed to explain some or all features observed, ranging from isolated resonances,<sup>5-7</sup> parity-dependent optical potentials,<sup>8</sup> channel-coupling to the excited states of the target nucleus,<sup>9</sup> and imaginary optical potentials calculated microscopically from single-particle transfers.<sup>10</sup> None of these models is able to explain all or even a large part of data.

Because of the presence of anomalies in both elastic and  $\alpha$ -transfer reactions, an attractive explanation could be the coupling between elastic channel and the  $\alpha$ -transfer channels. A first attempt<sup>11</sup> to include this coupling has been applied to the  $^{24}\text{Mg} + ^{12}\text{C}$  elastic scattering at 40 MeV. The coupling to the  $^{24}\text{Mg}(^{12}\text{C}, ^{16}\text{O})^{20}\text{Ne}$  reaction was described in the framework of Frahn's closed formalism<sup>12</sup> and a good agreement with data was obtained. The  $^{24}\text{Mg}(^{16}\text{O}, ^{16}\text{O})^{24}\text{Mg}$  angular distribution was explained through a molecular potential calculation<sup>13</sup> describing  $^{24}\text{Mg}$  as  $^{16}\text{O} + 2\alpha$ . In order to explain the anomalous back-angle excitation function of the  $^{28}\text{Si}(^{16}\text{O}, ^{16}\text{O})^{28}\text{Si}$  elastic scattering, the transfer of two and three  $\alpha$  particles was described in a semiclassical treatment<sup>14</sup> of the interplay between transfer process and absorption. The general trend of data is consistent with the calculated energy dependence.

In a recent work of Hussein and collaborators,<sup>15</sup> the coupling to  $\alpha$ -transfer channel has been explicitly taken into account by the evaluation of a dynamic  $\alpha$ -transfer polarization potential (DTPP) for the process  $^{16}\text{O} + ^{28}\text{Si} \rightarrow ^{12}\text{C} + ^{32}\text{S} \rightarrow ^{16}\text{O} + ^{28}\text{Si}$  and the back-angle elastic scattering of  $^{16}\text{O} + ^{28}\text{Si}$  has been reproduced with the polarization potential added to the  $E-18$  optical potential.

The aim of this work is to evaluate the effect of the dynamic  $\alpha$ -transfer polarization potential, not only on the elastic channel, but simultaneously on  $\alpha$ -transfer and inelastic channels also, and compare with experimental

data. This comparison was made for the following reaction channels at  $E_{c.m.} = 27.8$  MeV:



In order to have complete experimental angular distributions of all these channels, we measured the inelastic angular distribution in the forward and intermediate angle region ( $40^\circ \leq \vartheta_{c.m.} \leq 100^\circ$ ) and the angular distributions of the  $^{24}\text{Mg}(^{16}\text{O}, ^{20}\text{Ne})^{20}\text{Ne}$  reaction leading to the ground state and excited states of the final nuclei. We also completed in the forward and intermediate angle region ( $40^\circ \leq \vartheta \leq 100^\circ$ ) the elastic and  $\alpha$ -stripping angular distributions measured by Paul and collaborators.<sup>4</sup>

We also measured excitation functions<sup>16</sup> for the reactions  $^{24}\text{Mg}(^{16}\text{O}, ^{20}\text{Ne})^{20}\text{Ne}_{g.s.}$ ,  $^{24}\text{Mg}(^{16}\text{O}, ^{20}\text{Ne}(2^+))^{20}\text{Ne}$  at  $\vartheta_{c.m.} = 90^\circ$  and  $^{24}\text{Mg}(^{16}\text{O}, ^{12}\text{C})^{28}\text{Si}_{g.s.}$  and  $^{24}\text{Mg}(^{16}\text{O}, ^{12}\text{C})^{28}\text{Si}(2^+)$  at  $\vartheta_{c.m.} = 70^\circ$ . These excitation functions are also being analyzed in the framework of the DTPP formalism.

The  $^{24}\text{Mg}(^{16}\text{O}, \text{Ne})^{20}\text{Ne}_{g.s.}$  angular distribution at 27.8 MeV presents a strong minimum at  $90^\circ$  (Fig. 3), and its excitation function, measured at  $90^\circ$ , shows also a strong minimum at 27.8 MeV.<sup>16</sup> This result cannot be understood by the isolated resonance with  $J=20$ , which was used to explain<sup>7</sup> the structures present at 27.8 MeV in the  $^{24}\text{Mg}(^{16}\text{O}, ^{12}\text{C})^{28}\text{Si}_{g.s.}$  excitation functions at  $0^\circ$ ,  $90^\circ$ , and  $180^\circ$ , since the contribution of an even single  $l$  value in the symmetrized amplitude, should produce a maximum at  $90^\circ$  in the  $^{20}\text{Ne} + ^{20}\text{Ne}$  channel. It seems also difficult to explain why a resonance, which is present in the  $^{24}\text{Mg} + ^{16}\text{O}$  channel and  $^{12}\text{C} + ^{28}\text{Si}$  channel, should be absent in the  $^{20}\text{Ne} + ^{20}\text{Ne}$  channel, if the resonant partial wave, near to the grazing  $l$  value ( $lg=16$ ) would not be absorbed. So a complete description of the anomalies at 27.8 MeV has to take into account these new experimental facts.

The dynamic  $\alpha$ -transfer polarization potential, describing the coupling between the elastic and the  $\alpha$ -stripping

channel, was calculated and introduced into a DWBA code and its effect on the elastic, inelastic, and transfer cross sections was calculated. The general agreement between measured angular distributions and calculations is good, indicating that the  $\alpha$ -transfer coupling can have an important contribution to explain the back-angle anomalies. However the DTPP, which produces a localized  $l$  window in the scattering matrix, also fails to explain the minimum at  $90^\circ$  in the  $^{20}\text{Ne} + ^{20}\text{Ne}$  channel.

## II. EXPERIMENTAL METHOD AND RESULTS

The angular distributions of elastic, inelastic, and transfer reactions of the system  $^{16}\text{O} + ^{24}\text{Mg}$  were measured using an  $^{16}\text{O}$  beam accelerated to  $E_{\text{lab}} = 46.5$  MeV by the São Paulo Pelletron Accelerator. Targets of isotopically enriched  $^{24}\text{Mg}$  were evaporated on  $^{12}\text{C}$  backing. Three sets of  $\Delta E$ - $E$  telescopes were used, the  $E$  detectors being standard Si surface barrier detectors and the  $\Delta E$  detectors proportional gas counters. A thin layer of Bi was evaporated on the  $^{12}\text{C}$  backings before the  $^{24}\text{Mg}$  evaporation and the Rutherford scattering of  $^{16}\text{O}$  on Bi provided a practical way to normalize the data. A monitor placed at  $15^\circ$  with respect to the beam permitted us to calculate the ratio of  $^{24}\text{Mg}$  to Bi target thickness to obtain absolute cross sections for all measured processes. The energy resolution at all angles was sufficient to separate the elastic peak from inelastic peaks.

We measured at  $E_{\text{c.m.}} = 27.8$  MeV the angular distributions of the  $^{24}\text{Mg}(^{16}\text{O}, ^{20}\text{Ne})^{20}\text{Ne}$  reactions, leading to the ground state and excited states of final nuclei, and completed in the forward and intermediate angle region ( $40^\circ \leq \vartheta_{\text{c.m.}} \leq 110^\circ$ ) the inelastic, elastic, and  $\alpha$ -stripping angular distributions, measured by Paul and collaborators.<sup>4</sup>

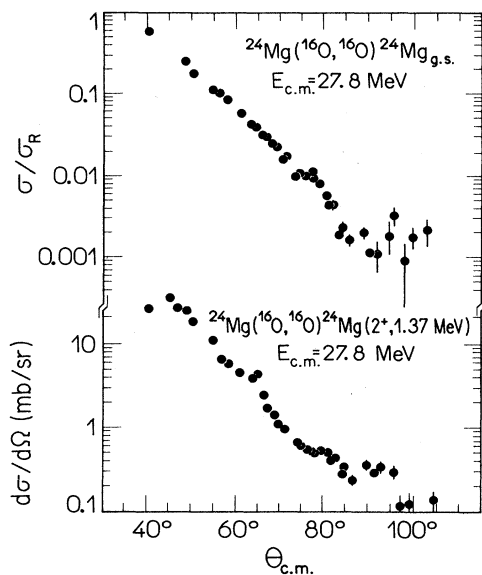


FIG. 1. Angular distributions of the  $^{24}\text{Mg}(^{16}\text{O}, ^{16}\text{O})^{24}\text{Mg}$  elastic scattering and  $^{24}\text{Mg}(^{16}\text{O}, ^{16}\text{O})^{24}\text{Mg}(2^+, 1.37$  MeV) inelastic scattering.

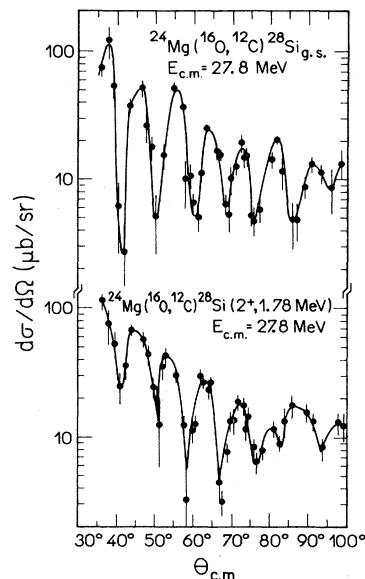


FIG. 2. Angular distributions of the  $^{24}\text{Mg}(^{16}\text{O}, ^{12}\text{C})^{28}\text{Si}(0^+, \text{g.s.})$  and  $^{24}\text{Mg}(^{16}\text{O}, ^{12}\text{C})^{28}\text{Si}(2^+, 1.78$  MeV) reactions. The solid line is only to guide the eye.

In Fig. 1 we present our elastic and inelastic angular distributions. In Fig. 2 we present our transfer reaction  $^{24}\text{Mg}(^{16}\text{O}, ^{12}\text{C})^{28}\text{Si}_{\text{g.s.}}$  and  $^{24}\text{Mg}(^{16}\text{O}, ^{12}\text{C})^{28}\text{Si}(2^+, 1.78$  MeV) angular distributions, and in Fig. 3 we show our data on  $^{24}\text{Mg}(^{16}\text{O}, ^{20}\text{Ne})^{20}\text{Ne}$ , leading, respectively, to the  $^{20}\text{Ne}$  ground state, one  $^{20}\text{Ne}$  excited to the  $2^+$ , 1.63 MeV

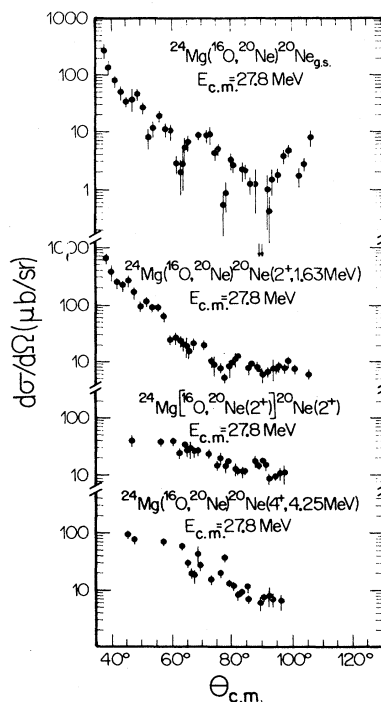


FIG. 3. Angular distributions  $^{24}\text{Mg}(^{16}\text{O}, ^{20}\text{Ne})^{20}\text{Ne}(0^+, \text{g.s.})$ ,  $^{24}\text{Mg}(^{16}\text{O}, ^{20}\text{Ne})^{20}\text{Ne}(2^+, 1.63$  MeV),  $^{24}\text{Mg}(^{16}\text{O}, ^{20}\text{Ne}(2^+, 1.63$  MeV)  $^{20}\text{Ne}(2^+, 1.63$  MeV), and  $^{24}\text{Mg}(^{16}\text{O}, ^{20}\text{Ne})^{20}\text{Ne}(4^+, 4.25$  MeV) reactions.

state, both  $^{20}\text{Ne}$  excited to the  $2^+$  state, one  $^{20}\text{Ne}$  excited to the  $4^+$ , 4.25 MeV state.

Our elastic scattering and ( $^{16}\text{O}, ^{12}\text{C}$ ) data agree well with the measurements of Paul<sup>4</sup> from  $\vartheta_{\text{c.m.}} = 35^\circ$  to  $55^\circ$ . From  $55^\circ$  to  $100^\circ$  our data are more precise and present more structures. The  $^{24}\text{Mg}(^{16}\text{O}, ^{20}\text{Ne})^{20}\text{Ne}_{\text{g.s.}}$  angular distribution shown in Fig. 3 presents strong oscillations and a symmetry around  $90^\circ$ , with a strong minimum at  $90^\circ$ .

### III. ANALYSIS OF THE DATA

#### A. The dynamic $\alpha$ -transfer polarization potential

Hussein and collaborators<sup>15</sup> define the dynamic  $\alpha$ -transfer polarization potential,  $V_{\text{pol}}$ , to be the potential which reproduces, to first order, the correction to the elastic scattering  $T$  matrix, arising from an explicit consideration of the transfer process  $0 \rightarrow 1 \rightarrow 0$ , namely

$$\Delta T_{00}^{(1)}(\mathbf{k}, \mathbf{k}') = \langle \varphi_0; \chi^{(-)}(\mathbf{k}'_0) | H_{01} G_1^{(+)} H_{10} | \varphi_0; \chi_0^{(+)}(\mathbf{k}_0) \rangle \quad (1)$$

$$\equiv \langle \chi_0^{(-)}(\mathbf{k}'_0) | V_{\text{pol}} | \chi_0^{(+)}(\mathbf{k}_0) \rangle, \quad (2)$$

where  $\chi^{(\pm)}$  are the waves distorted by the background strong absorption interaction,  $\varphi_0$  is the intrinsic ground state of the combined system,  $H_{01}$  and  $H_{10}$  are the appropriate transfer coupling interactions, and  $G_1^{(+)}$  is the unperturbed distorted Green function describing the propagation in channel 1, in the presence of the strong absorption potential. The DTPP can be expanded in partial waves and from this nonlocal DTPP a trivially equivalent local potential is defined through

$$\bar{V}_{\text{pol}}^l(r) f_l^0(kr) \equiv \int_0^\infty dr' V_{\text{pol}}^l(r, r') f_l^0(kr'), \quad (3)$$

where  $f_l^0(kr)$  is the distorted partial wave function.

One finds that using the no recoil (NR) and zero range (ZR) approximations, and including a factor of 2 due to off-shell corrections,<sup>17</sup> the trivially equivalent local potential  $\bar{V}_{\text{pol}}$  can be written as

$$\bar{V}_{\text{pol}}^l(r) = C_l(E) F(r), \quad (4)$$

where  $F(r)$  is the form factor of the  $\alpha$ -transfer reaction and  $C_l(E)$  is given by

$$C_l(E) = A \left[ -\frac{4i\mu_1}{\hbar^2 k_1} \frac{(I_l^{01}(k_0, k_1))^2}{I_l^{00}(k_0) S_{l,1}^N(k_1)} \right], \quad (5)$$

where  $A$  contains the spectroscopic amplitudes, normalization due to recoil and finite-range effects,  $I_l^{01}$  is the transfer radial integral,  $I_l^{00}$  is the elastic radial integral, and  $S_{l,1}^N$  are the unperturbed nuclear elastic scattering matrix elements in the transfer channel.

TABLE I. Optical potential parameters.

Potential $V$ (MeV)	$r_r$ (fm)	$a_r$ (fm)	$W$ (MeV)	$r_l$ (fm)	$a_l$ (fm)
ANL2	10.0	1.452	0.345	23.0	1.272 0.376

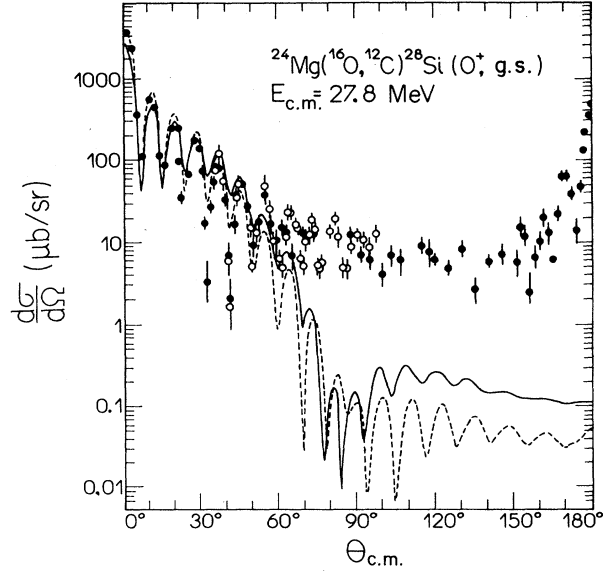


FIG. 4. Full experimental angular distribution of the  $^{24}\text{Mg}(^{16}\text{O}, ^{12}\text{C})^{28}\text{Si}(0^+, \text{g.s.})$  reaction, our data are indicated by open circles and data of Paul *et al.* (Ref. 4) with solid dots. The continuous line is the cross section calculated by PTOLEMY and the dashed line is the calculation by DWPOL, using the potential ANL2 in both channels. The calculations are normalized to experimental data at forward angles.

#### B. Applications to the system $^{24}\text{Mg} + ^{16}\text{O}$ at $E_{\text{c.m.}} = 27.8$ MeV

##### 1. Details of the calculation

We apply the formalism of DTPP to the system  $^{24}\text{Mg} + ^{16}\text{O}$ , assuming the  $\alpha$ -transfer process  $^{24}\text{Mg} + ^{16}\text{O} \rightarrow ^{28}\text{Si} + ^{12}\text{C} \rightarrow ^{24}\text{Mg} + ^{16}\text{O}$  as a basis for our coupled-channels discussion. The corresponding polarization potential is constructed with channel 0 being  $^{24}\text{Mg} + ^{16}\text{O}$  and channel 1 being  $^{28}\text{Si} + ^{12}\text{C}$  and all partici-

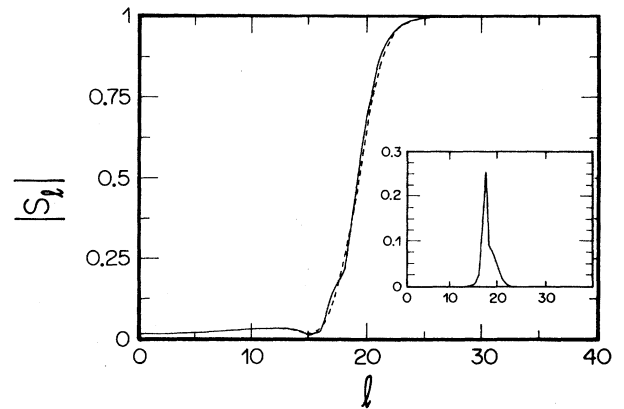


FIG. 5. The solid line indicates the modulus of the perturbed scattering matrix  $|S_{l,0}^p|$  and the dashed line of the unperturbed scattering matrix  $|S_{l,0}^0|$ , the inset indicates the modulus of the difference  $|S_{l,0}^p - S_{l,0}^0|$ .

pating nuclei are in their respective ground states. We developed a DWBA code named DWPOL, based on DWUCK, which used the no-recoil and zero-range approximations in order to calculate  $\bar{V}_{\text{pol}}$  and the cross sections.

It is a well-known fact that zero-range and no-recoil calculations fail badly for heavy-ion  $\alpha$ -transfer reactions. The effect of ZR and NR approximations depends on the optical potential used in the incoming and outgoing channels. For some potentials the effect reduces to a simple disagreement in absolute value presenting very similar angular dependence.

In order to estimate the effect of ZR and NR approximations, we compared the transfer differential cross section calculated by DWPOL (without  $\bar{V}_{\text{pol}}$ ) and by the full finite-range DWBA code PTOLEMY for the reaction  $^{24}\text{Mg}(^{16}\text{O}, ^{12}\text{C})^{28}\text{Si}_{\text{g.s.}}$ , using the optical potential obtained by Tabor,<sup>19</sup> called ANL2 (see Table I) in the incoming and outgoing channels. The bound-state wave functions are calculated in the usual way, adjusting the depth of a Woods-Saxon well with  $R = 1.25 A_T^{1/3}$  fm and  $a = 0.65$  fm, in order to reproduce the separation energies. The transferred four-nucleon cluster (called an  $\alpha$ -particle hereafter) is assumed to be in an internal 1S state.

Both calculations give very similar angular distributions, as can be seen in Fig. 4, resulting in a constant normalization factor which takes into account the recoil and finite-range effects.

The angular distributions of the other transfer reactions ( $\alpha$  stripping and  $\alpha$  pickup) have also been compared through DWPOL and PTOLEMY calculations, and in all cases the "exact" and NR and ZR angular distributions had very similar angular dependence, and the normalization factor was the very same in all cases.

In view of this result we concluded that the NR and ZR calculations, with ANL2 potential, should be safely used, when conveniently corrected by the appropriate normalization factor.

The calculations were performed in the following steps.

(a) The radial integrals  $I_l^{01}$  and  $I_l^{00}$  and the scattering matrix  $S_{l,1}^N$  were calculated by the DWBA code DWPOL together with the  $\alpha$ -transfer form factor  $F(r)$ , computing subsequently the polarization potential  $\bar{V}_{\text{pol}}$ .

(b) The full normalization of  $\bar{V}_{\text{pol}}$ , including also spectroscopic factors of the reaction  $^{24}\text{Mg}(^{16}\text{O}, ^{12}\text{C})^{28}\text{Si}_{\text{g.s.}}$ , was obtained comparing the experimental differential cross section of this reaction at forward angles with the DWPOL calculated transfer cross section.

(c) The normalized  $\bar{V}_{\text{pol}}$  is added to the optical potential and the radial Schrödinger equation is solved, generating the exact, perturbed wave function in the elastic channel  $\bar{\psi}_l^0(r)$ . From this wave function we calculated the perturbed scattering matrix  $\bar{S}_{l,0}$ , which is compared in Fig. 5 with the unperturbed scattering matrix  $S_{l,0}$ . The slight difference between them is localized around the grazing angular momentum, as can be seen in the inset of Fig. 5, where the difference  $|\bar{S}_{l,0} - S_{l,0}|$  is shown.

(d) This exact wave function is used in DWPOL to calculate the elastic angular distribution, the inelastic excitation cross sections, and the transfer cross sections for all transfer processes, namely

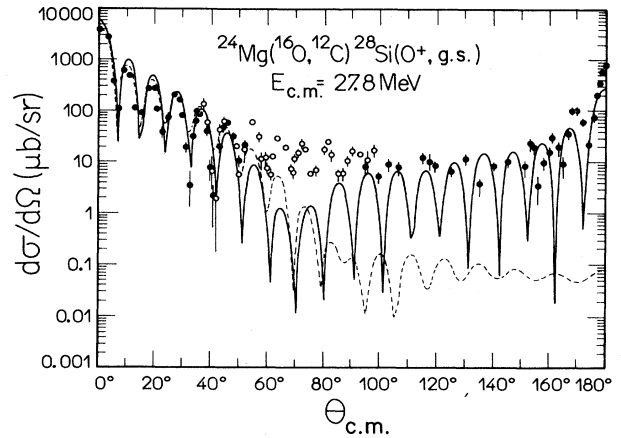
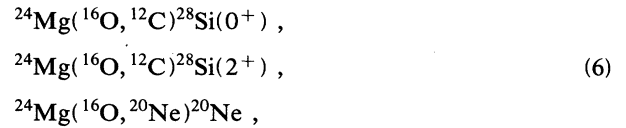


FIG. 6. Experimental angular distribution of  $^{24}\text{Mg}(^{16}\text{O}, ^{12}\text{C})^{28}\text{Si}(0^+, \text{g.s.})$  reaction, our data are the open circles and the data of Paul (Ref. 4) the solid dots. The continuous line is the cross section calculated in the presence of  $\bar{V}_{\text{pol}}$  and the dashed line without  $\bar{V}_{\text{pol}}$ .



including the effect of  $\bar{V}_{\text{pol}}$  in all of these processes. The same code permitted us to calculate these cross sections without including  $\bar{V}_{\text{pol}}$ , in order to compare both calculations.

## 2. Calculations of the cross sections for the $^{24}\text{Mg} + ^{16}\text{O}$ system, including the polarization potential

a. The reaction  $^{24}\text{Mg}(^{16}\text{O}, ^{16}\text{O})^{24}\text{Mg}_{\text{g.s.}}$ . The differential transfer cross sections were calculated without and in the

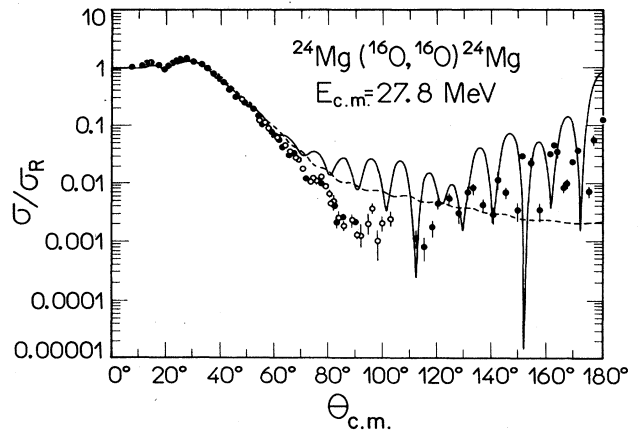


FIG. 7. Experimental angular distribution of  $^{24}\text{Mg}(^{16}\text{O}, ^{16}\text{O})^{24}\text{Mg}$  elastic scattering, our data are the open circles and the data of Paul (Ref. 4) and the solid dots. The continuous line is the cross section calculated in the presence of  $\bar{V}_{\text{pol}}$  and the dashed line without  $\bar{V}_{\text{pol}}$ .

presence of  $\bar{V}_{\text{pol}}$  and normalized to experimental data at forward angles.

The effect of  $\bar{V}_{\text{pol}}$  in the transfer angular distribution is small at forward angles, but produces strong oscillations and rise in the backward-angle region. However, its effect in the backward angles is still smaller than the experimental cross section. If we multiply  $\bar{V}_{\text{pol}}$  by an additional factor of 1.9 the calculated transfer cross section reproduces well the backward rise in the experimental data, as can be verified in Fig. 6, where we compare the complete experimental angular distribution of  $^{24}\text{Mg}(^{16}\text{O}, ^{12}\text{C})^{28}\text{Si}_{\text{g.s.}}$ , including our data (open circles) and that of Paul<sup>4</sup> (solid dots) with the calculated transfer cross section in the presence of  $\bar{V}_{\text{pol}}$  (continuous line) and without  $\bar{V}_{\text{pol}}$  (dashed line). This additional normalization factor can be attributed to the off-shell effects, whose influence can modify the  $\bar{V}_{\text{pol}}$  by a factor ranging from 1 to 4.<sup>17</sup> The reason to perform the final normalization of  $\bar{V}_{\text{pol}}$  adjusting the backward cross section of the  $^{24}\text{Mg}(^{16}\text{O}, ^{12}\text{C})^{28}\text{Si}_{\text{g.s.}}$  is that we assume that the backward anomaly in this channel is due exclusively to the dynamical  $\alpha$ -transfer polarization potential  $\bar{V}_{\text{pol}}$ . In the calculations of other channels, this same normalization of  $\bar{V}_{\text{pol}}$  will be maintained.

*b. Elastic scattering  $^{24}\text{Mg}(^{16}\text{O}, ^{16}\text{O})^{24}\text{Mg}$ .* The  $\bar{V}_{\text{pol}}$  is included in the Schrödinger equation, together with the optical potential ANL2. The elastic cross section, calculated in the presence of these potentials, is shown in Fig. 7 together with experimental data. The calculation provides the backward rise, which is somewhat overestimated. Many attempts were performed, using many different optical potentials, in order to reduce the effect in the elastic channel, without reducing in the  $\alpha$ -transfer channel, but in no way could we change this behavior. This fact can be an indication that the coupling to other channels (inelastic,  $\alpha$  pickup), which are neglected in this calculation, are more important in the elastic channel than in the  $\alpha$ -stripping ground-state transition.

*c. Inelastic scattering  $^{24}\text{Mg}(^{16}\text{O}, ^{16}\text{O})^{24}\text{Mg}(2^+, 1.37 \text{ MeV})$ .* The inelastic cross section was calculated by DWPOL, using collective nuclear form factors, given by the derivative of the optical potential

$$F_N(r) = \delta_2^N \left[ V \frac{df_R(r)}{dr} + iW \frac{df_I(r)}{dr} \right], \quad (7)$$

where  $\delta_2^N = \beta_2^N R_N$  is the nuclear deformation length and the nuclear optical potential is

$$U(r) = -Vf_R(r) - iWf_I(r). \quad (8)$$

The Coulomb form factor is

$$F_C(r) = \frac{4\pi}{5} \frac{Ze[B(E2\uparrow)]^{1/2}}{r^3} = \frac{3}{5} \frac{Z^2 e^2 R_C^2 \beta_2^C}{r^3}. \quad (9)$$

Using  $R_C = r_{0C} A_T^{1/3}$  with  $r_{0C} = 1.495 \text{ fm}$  and the adopted value of  $B(E2\uparrow) = 430 e^2 \text{ fm}^4$ , we obtain  $\beta_2^C = 0.3897$  and  $\delta_2^C = \beta_2^C R_C = 1.68$ . The nuclear deformation length  $\delta_2^N = \beta_2^N R$ , obtained in other inelastic scattering measurements on  $^{24}\text{Mg}$ ,<sup>20,21</sup> is around 1.5 and 1.6. We also performed coupled-channels calculations with the code ECIS,

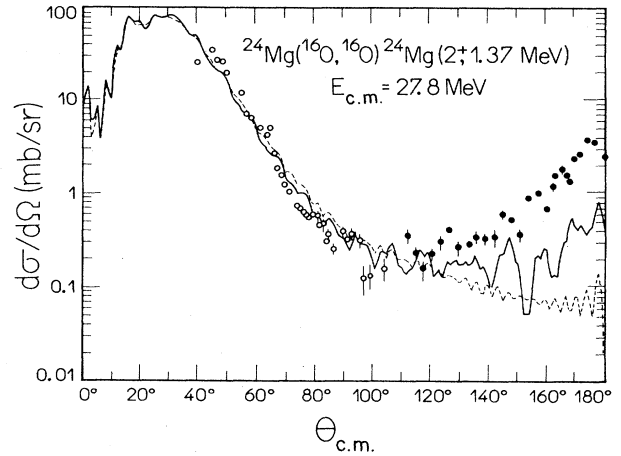


FIG. 8. Experimental angular distribution of  $^{24}\text{Mg}(^{16}\text{O}, ^{16}\text{O})^{24}\text{Mg}(2^+, 1.37 \text{ MeV})$  inelastic scattering, our data are the open circles and the data of Paul (Ref. 4) are the solid dots. The continuous line is the cross section calculated in the presence of  $\bar{V}_{\text{pol}}$  and the dashed line without  $\bar{V}_{\text{pol}}$ .

where we obtained a good accord with our forward inelastic data, using the ANL2 potential,  $\beta_2^C = 0.3897$  and  $\beta_2^N R_N = 1.5$ . However, when these deformation parameters are used in DWBA approximation the agreement is much worse. In order to get a good fit of the data using DWPOL, we have to increase  $\beta_2^C$  to 0.542 and reduce  $\delta_2^N$  to 0.862. The full inelastic experimental angular distribution and the calculations with  $\bar{V}_{\text{pol}}$  (continuous line) and without  $\bar{V}_{\text{pol}}$  (dashed line) are shown in Fig. 8. The deformation parameters used in this calculation are  $\delta_2^N = 0.862$  and  $\beta_2^C = 0.542$ . The effect of  $\bar{V}_{\text{pol}}$  is again small at forward angles, but produces an increase and strong oscillations at the backward angles. However, the

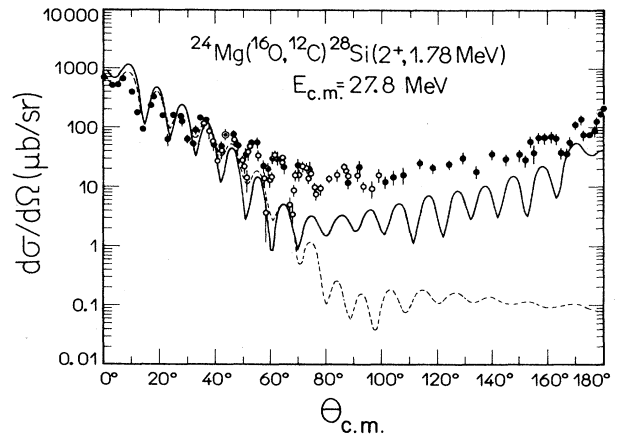


FIG. 9. Experimental angular distribution of  $^{24}\text{Mg}(^{16}\text{O}, ^{12}\text{C})^{28}\text{Si}(2^+, 1.78 \text{ MeV})$  reaction, our data are the open circles and the data of Paul (Ref. 4) are the solid dots. The continuous line is the cross section calculated in the presence of  $\bar{V}_{\text{pol}}$  and the dashed line without  $\bar{V}_{\text{pol}}$ .

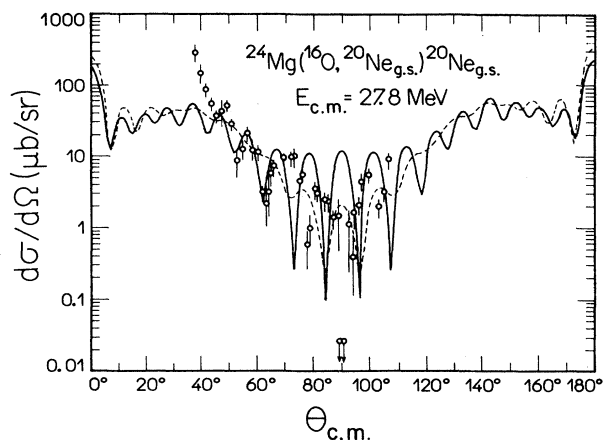


FIG. 10. Experimental angular distribution of  $^{24}\text{Mg}(^{16}\text{O}, ^{20}\text{Ne})^{20}\text{Ne}(0^+, \text{g.s.})$  reaction. The continuous line is the cross section calculated in the presence of  $\bar{V}_{\text{pol}}$  and the dashed line without  $\bar{V}_{\text{pol}}$ .

backward cross section is still somewhat underestimated.

d. *The reaction  $^{24}\text{Mg}(^{16}\text{O}, ^{12}\text{C})^{28}\text{Si}(2^+, 1.78 \text{ MeV})$ .* The transfer cross sections, calculated without and in the presence of  $\bar{V}_{\text{pol}}$  and normalized to experimental data at forward angles, are shown in Fig. 9, together with experimental angular distribution. The calculation without  $\bar{V}_{\text{pol}}$  (dashed curve) reproduces well the forward angle cross section but fails completely at backward angles. The effect of the inclusion of  $\bar{V}_{\text{pol}}$  again is small at forward angles and produces oscillations and rise at backward angles, which are, however, underestimated.

e. *The reaction  $^{24}\text{Mg}(^{16}\text{O}, ^{20}\text{Ne})^{20}\text{Ne}_{\text{g.s.}}$*  The outgoing particles are identical and this fact implies, in two modifications in the calculations of the transfer cross section,<sup>22</sup> that there is a double counting in the detection, because the detector cannot distinguish between  $^{20}\text{Ne}$  originating from target or projectile; and the outgoing wave function has to be symmetrized. The transfer cross

section, calculated in these conditions, can be written as

$$\frac{d\sigma}{d\Omega} = |f(\vartheta, \varphi) + f(\pi - \vartheta, \varphi + \pi)|^2,$$

where  $f(\vartheta, \varphi)$  is the transfer amplitude calculated without considering the identity of particles. Only even partial waves will contribute to the summed transfer amplitude and the cross section will be symmetrical around  $90^\circ$ .

We have calculated the transfer cross section without  $\bar{V}_{\text{pol}}$ , taking into account both effects affecting identical particles, and again normalizing the calculation to the mean behavior of forward-angle experimental data. The calculation, presented in Fig. 10 as a dashed line, produces a maximum at  $90^\circ$ , in disaccord with experimental result, and almost no oscillations at forward and backward angles, showing even a smooth bell shape, with maximum at  $\vartheta_{\text{gr}} \sim 40^\circ$ , due to negative  $Q$  value of the reaction ( $-4.58 \text{ MeV}$ ). The effect of inclusion of  $\bar{V}_{\text{pol}}$  in the calculation is to introduce oscillations at forward and backward angles which agree well with experimental data. However, the maximum at  $90^\circ$  remains even with  $\bar{V}_{\text{pol}}$ , indicating that the experimental minimum is not related to this  $\alpha$ -transfer coupling.

The excitation function of this transition measured<sup>16</sup> at  $90^\circ$  also presents a strong minimum at this energy (27.8 MeV). This fact has also been observed in other cases of identical particle scattering, as the elastic scattering  $^{12}\text{C}(^{12}\text{C}, ^{12}\text{C})^{12}\text{C}$  at some energies.<sup>23,24</sup> We are investigating the origin of this minimum.

f. *The reactions  $^{24}\text{Mg}(^{16}\text{O}, ^{20}\text{Ne})^{20}\text{Ne}$  leading to excited states ( $2^+$  at 4.25 MeV) in  $^{20}\text{Ne}$ .* We performed calculations with PTOLEMY for these reactions and verified that the cross section for the reaction  $^{24}\text{Mg}(^{16}\text{O}, ^{20}\text{Ne})^{20}\text{Ne}_{\text{g.s.}}$  is much higher than for the reaction  $^{24}\text{Mg}(^{16}\text{O}, ^{20}\text{Ne})^{20}\text{Ne}^*$ . The spectroscopic factors for  $^{16}\text{O} + \alpha \rightarrow ^{20}\text{Ne}^*$  are also higher than for  $^{24}\text{Mg} - \alpha \rightarrow ^{20}\text{Ne}^*$ . As a consequence, the experimental angular distributions for the excitation of one  $^{20}\text{Ne}$  to its  $2^+$  or  $4^+$  states, respectively, can be considered essentially as

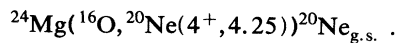
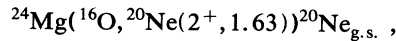
TABLE II. Comparison of relative theoretical spectroscopic factors of the reactions  $^{24}\text{Mg}(^{16}\text{O}, ^{12}\text{C})^{28}\text{Si}$  and  $^{24}\text{Mg}(^{16}\text{O}, ^{20}\text{Ne})^{20}\text{Ne}$  with our relative normalization factors  $N$ , defined in text.  $S_1$  refers to target spectroscopic factors and  $S_2$  to projectile spectroscopic factors,  $S_1 S_2$  refers to the reactions indicated and  $S_1 S_2 / S_1 S_2(^{16}\text{O}, ^{12}\text{C})_{\text{g.s.}}$  are the reaction spectroscopic factors normalized to the ground-state transition of the  $(^{16}\text{O}, ^{12}\text{C})$  reaction.  $N$  are our relative normalization factors. The theoretical spectroscopic factors  $S_1$  and  $S_2$  were normalized such that  $S_\alpha = 1$  for  $^{16}\text{O}_{\text{g.s.}} + \alpha \rightarrow ^{20}\text{Ne}_{\text{g.s.}}$ .

$S_1(^{24}\text{Mg} + \alpha \rightarrow ^{28}\text{Si}(J^\pi))$	$S_2(^{12}\text{C} + \alpha \rightarrow ^{16}\text{O})$	$S_1 S_2$	$\frac{S_1 S_2}{S_1 S_2(^{16}\text{O}, ^{12}\text{C})_{\text{g.s.}}}$	$N$
$J^\pi$				
$0^+$	0.41 <sup>a</sup>	1.62 <sup>b</sup>	0.664	1
$2^+$	0.094 <sup>a</sup>	1.62 <sup>b</sup>	0.152	0.23
$S_1(^{24}\text{Mg} - \alpha \rightarrow ^{20}\text{Ne}(J^\pi))$	$S_2(^{16}\text{O} + \alpha \rightarrow ^{20}\text{Ne})$			
$J^\pi$				
$0^+$	0.35 <sup>a</sup>	1.0	0.35	0.52

<sup>a</sup>Reference 25.

<sup>b</sup>Calculations of H. Yoshida, quoted in Ref. 26.

projectile excitation reaction, as



In DWPOL the projectile excitation cannot be taken into account and for these reasons, we cannot calculate at the present stage the effect of  $\bar{V}_{\text{pol}}$  on the reactions leading to excited states of  $^{20}\text{Ne}$  in these sections.

g. *Spectroscopic information.* In order to show that our results are quantitatively consistent, we compared our relative normalization  $N$  (defined as the normalization factor of the transition considered determined at forward angles, divided by the normalization factor of the  $\alpha$ -stripping ground-state transition), with the ratio of the theoretical spectroscopic factors corresponding to these transitions. In Table II we show the theoretical  $\alpha$ -spectroscopic factors  $S_1$  and  $S_2$ , for the target and projectile nuclei involved in these reactions,<sup>25,26</sup> normalized relative to the  $^{20}\text{Ne}_{\text{g.s.}} \rightarrow ^{16}\text{O}_{\text{g.s.}} + \alpha$  spectroscopic factor. The spectroscopic factors of the reactions are also presented in the third column of Table II as products of target and projectile spectroscopic factors. In the fourth column we show the relative spectroscopic factors of

these reactions, normalized to the ground-state transition of the ( $^{16}\text{O}, ^{12}\text{C}$ ) reaction. In the fifth column we show our relative normalization factors  $N$ , which are in excellent agreement with the relative theoretical spectroscopic factors of these reactions.

#### IV. CONCLUSIONS

We have calculated the dynamic  $\alpha$ -transfer polarization potential  $\bar{V}_{\text{pol}}$  and introduced it into our elastic, inelastic, and transfer calculations in order to estimate its effects on the back-angle anomalies observed in many channels of the  $^{24}\text{Mg} + ^{16}\text{O}$  system. The coupling between the elastic and  $\alpha$ -stripping channel explains in a fairly quantitative way the anomalies observed, overestimating the effect in the elastic channel and somewhat underestimating in some other channels. This fact can be an indication that other channel couplings can also be important and should be taken into account.

#### ACKNOWLEDGMENTS

We would like to thank Prof. M. S. Hussein and Prof. L. C. Gomes for very fruitful discussions. This work was supported by FINEP and CNPq.

- 
- <sup>1</sup>P. Braun-Munzinger and J. Barrette, *Phys. Rep.* **87**, 209 (1982).  
<sup>2</sup>J. Barrette and S. Kahana, *Comment Nucl. Part. Phys.* **9**, 67 (1980).  
<sup>3</sup>G. K. Gelbke, T. Awes, U. E. P. Berg, J. Barrette, M. J. Levine, and P. Braun-Munzinger, *Phys. Rev. Lett.* **41**, 1778 (1978).  
<sup>4</sup>M. Paul, S. J. Sanders, D. F. Geesaman, W. Henning, D. G. Kovar, C. Olmer, J. P. Schiffer, J. Barrette, and M. J. Levine, *Phys. Rev. C* **21**, 1802 (1980).  
<sup>5</sup>J. Barrette, M. J. Levine, P. Braun-Munzinger, G. M. Berkowitz, M. Gai, J. W. Harris, and C. M. Jachcinski, *Phys. Rev. Lett.* **40**, 445 (1978).  
<sup>6</sup>M. Paul, S. J. Sanders, J. Cseh, D. F. Geeseman, W. Henning, D. G. Kovar, C. Olmer, and J. P. Schiffer, *Phys. Rev. Lett.* **40**, 1310 (1978).  
<sup>7</sup>S. J. Sanders, M. Paul, J. Cseh, D. F. Geeseman, W. Henning, D. G. Kovar, R. Kozub, C. Olmer, and J. P. Schiffer, *Phys. Rev. C* **21**, 1810 (1980).  
<sup>8</sup>D. Dehnhard, V. Shkolnik, and M. A. Franey, *Phys. Rev. Lett.* **40**, 1549 (1978).  
<sup>9</sup>S. Kahana, G. Pollarolo, J. Barrette, A. Winther, and R. Broglia, *Phys. Lett.* **133B**, 283 (1983).  
<sup>10</sup>G. Pollarolo, R. A. Broglia, *Nuovo Cimento* **81**, 278 (1984).  
<sup>11</sup>R. Lichtenthäler Jr., A. Lépine-Szily, A. C. C. Villari, W. Mittag, V. J. G. Porto, and C. V. Acquardro, *Phys. Rev. C* **26**, 2487 (1982).  
<sup>12</sup>W. E. Frahn and M. S. Hussein, *Nucl. Phys.* **A346**, 237 (1980).  
<sup>13</sup>Guozhu He, Cheng-Qun Gao, and Ping-Zki Ning, *Phys. Rev. C* **30**, 534 (1984).  
<sup>14</sup>L. F. Canto, R. Donangelo, M. S. Hussein and A. Lépine-Szily, *Phys. Rev. Lett.* **51**, 95 (1983).  
<sup>15</sup>M. S. Hussein, A. N. Aleixo, L. F. Canto, P. Carrilho, R. Donangelo, and L. S. de Paula, *J. Phys. G* **13**, 967 (1987).  
<sup>16</sup>R. Lichtenthäler Filho, A. Lépine-Szily, A. C. C. Villari, J. Martins de Oliveira, Jr., M. M. Obuti, O. Portezan Filho, W. Sciani (unpublished).  
<sup>17</sup>T. Udagawa, K. S. Low, and T. Tamura, *Phys. Rev. C* **28**, 1033 (1983).  
<sup>18</sup>M. H. Macfarlane and S. C. Pieper, Argonne National Laboratory Report ANL76-11 (unpublished).  
<sup>19</sup>S. L. Tabor, D. F. Geesaman, W. Henning, D. G. Kovar, K. E. Rehm, and F. W. Prosser, Jr., *Phys. Rev. C* **17**, 2136 (1978).  
<sup>20</sup>W. Mittag, P. Charles, S. M. Lee, I. Badawy, B. Berthier, B. Fernandez, and J. Gastebois, *Nucl. Phys.* **A233**, 48 (1974).  
<sup>21</sup>J. S. Eck, D. O. Elliott, and W. J. Thompson, *Phys. Rev. C* **16**, 1020 (1977).  
<sup>22</sup>A. Messiah, *Mécanique Quantique* (Dunod, Paris, 1960), Chap. II, p. 514.  
<sup>23</sup>W. Reilly, R. Wieland, A. Gobbi, M. W. Saks, J. Maher, R. H. Siemseen, D. Mingay, and D. A. Bromley, *Nuovo Cimento* **13A**, 913 (1973).  
<sup>24</sup>R. M. Wieland, R. G. Stokstad, G. R. Satchler, and L. D. Rickertsen, *Phys. Rev. Lett.* **37**, 1458 (1976).  
<sup>25</sup>K. T. Hecht and D. Braunschweig, *Nucl. Phys.* **A244**, 365 (1975); J. P. Draayer, *ibid.* **A237**, 157 (1975).  
<sup>26</sup>C. Detraz, H. H. Duhm, and H. Hafner, *Nucl. Phys.* **A147**, 488 (1970).